Available online at www.sciencedirect.com

ScienceDirect

Original Research Paper

Experimental characterization of the 3D linear viscoelastic behavior of cold recycled bitumen emulsion mixtures

Andrea Graziani[*], Carlotta Godenzoni, Francesco Canestrari

Dipartimento di Ingegneria Civile, Edile e Architettura, Università Politecnica delle Marche, Ancona 60131, Italy

HIGHLIGHTS

- The 3D LVE behavior of HMA with 25% RAP can be simulated using the 2S2P1D model.
- At high reduced frequencies, HMA is stiffer than cold-recycled mixture.
- At low reduced frequencies, cold-recycled mixture is stiffer than HMA.
- E^* of cold-recycled mixture can be simulated using the Huet-Sayegh model.
- ν^* of cold-recycled mixture is almost constant and equal to 0.15.

ARTICLE INFO

ABSTRACT

Cold mixtures with bitumen emulsion are produced at ambient temperature, leading to substantial reductions of energy consumption and atmospheric emissions. In cold recycling applications, cement is normally used to improve the mixture performance. Thus, the rheological behavior of cold recycled mixtures is different from that of conventional hot mixtures because it is due to the interaction of fresh bitumen, aged bitumen and cementitious bonds. In this study, we investigated the three-dimensional (3D) linear viscoelastic (LVE) behavior of a cement-bitumen treated material (CBTM) mixture fabricated using bitumen emulsion and cement. For comparison, we also investigated the 3D LVE behavior of hot-mix asphalt containing 25% of reclaimed asphalt and fabricated using polymer-modified binder. Sinusoidal axial tests on cylindrical specimens, were carried out at various temperatures (from 0 °C to 50 °C) and frequencies (from 0.1 to 12 Hz). The complex Young's modulus E^* and the complex Poisson's ratio ν^* were determined through the measurement of axial and transverse strain. We show that when considering E^*, CBTM mixtures may be considered thermo-rheologically simple and the Huet-Sayegh model can be used to simulate the frequency−temperature dependence. On the other hand, when considering ν^* the behavior of CBTM mixtures is very different from that of hot mix asphalt. In particular, its absolute value is almost constant and very close to 0.15.

* Corresponding author. Tel.: +39 071 220 4507.
E-mail addresses: a.graziani@univpm.it (A. Graziani), f.canestrari@univpm.it (F. Canestrari).
Peer review under responsibility of Periodical Offices of Chang'an University.

J. Traffic Transp. Eng. (Engl. Ed.) 2019; 6 (4): 324—336

325

1. Introduction

Cold bitumen emulsion (CBE) paving technologies allow the production of paving mixtures at ambient temperature, leading to substantial reductions of energy consumption and atmospheric emissions, with respect to hot and warm asphalt technologies (Goyer et al., 2012; Nikolaides, 1994). Sustainable and cost-effective mixtures are obtained applying CBE technologies to cold in-place and in-plant recycling of asphalt pavements (Giani et al., 2015; Turk et al., 2016).

Cold recycled mixtures (CRM) with bitumen emulsion are produced using up to 100% reclaimed asphalt pavement (RAP) aggregate (Asphalt Academy, 2009; Thompson et al., 2009). Their mechanical performance is normally improved by using hydraulic binders like ordinary Portland cement, composite cements or other supplementary cementitious materials (Brown and Needham, 2000; Dolzycki et al., 2017). Depending on the aggregate quality and on the dosages of bitumen emulsion and cement, the mechanical behavior of CRM can be extremely variable. In particular, cement-bitumen treated materials (CBTM) are produced with a cement dosage up to 3% with respect to the dry mass of aggregate and are characterized by a bitumen-to-cement ratio close to 1. This leads to a mixture with high strength and stiffness, which is used for building sub-base and base courses of high-traffic highways (Bocci et al., 2011; Grilli et al., 2012; Stimilli et al., 2013).

CBTM mixtures are time- and temperature-dependent materials. Thus, similar to hot-mix asphalt (HMA) mixtures, the complex modulus can be used to characterize their one-dimensional (1D) linear viscoelastic (LVE) behavior. In this regard, Stimilli et al. (2013) measured the complex modulus of CBTM with bitumen emulsion on both laboratory-compacted specimens and field cores. They showed that the time—temperature superimposition principle (TTSP) can be considered valid for the absolute value of the complex modulus and that master curves can be modelled using a 4-parameter sigmoidal equation. A similar approach was used by Schwartz et al. (2017) to model the dynamic modulus of a wide range CRM produced with bitumen emulsion and foamed bitumen. The master curve data suggests that CRM with foamed bitumen may be slightly stiffer at higher temperatures, whereas CRM with bitumen emulsion may be slightly stiffer at lower temperatures. Gandi et al. (2017) measured the complex modulus of CBTM mixtures with different contents of RAP. They used the 2S2P1D rheological model to simulate the thermo-rheological behavior and concluded that the amount of RAP does not have a strong influence on the phase angle. Graziani et al. (2018b) measured the complex modulus on cores extracted from a pavement test section where CBTM mixtures were fabricated using bitumen emulsion and foamed bitumen. The results confirmed the validity of the TTSP and were fitted using the Huet-Sayegh (HS) rheological model.

For both HMA and CBTM mixtures, even in the isotropic case, the measurement of two independent response functions is necessary to obtain a complete three-dimensional (3D) LVE characterization (Sauzeat and Di Benedetto, 2015; Tschoegl, 1989). Considering this background, in this study we investigated the 3D-LVE behavior of a CBTM mixture produced with bitumen emulsion and cement. Our main objective was to characterize their frequency and temperature dependence by measuring the complex Young's modulus E^* and, for the first time, the complex Poisson's ratio (PR) v^*. For comparison, we also investigated the 3D LVE behavior of a HMA mixture containing 25% of reclaimed asphalt and fabricated using polymer-modified binder.

The organization of this paper is as follow. In Section 2 we present the theoretical background for the 3D isotropic characterization of bituminous mixtures. In Section 3 we describe the experimental program which is based on sinusoidal compression tests performed on cylindrical specimens. In Section 4 we show the experimental results and analyze the rheological behavior of HMA and CBTM specimens using the 2S2P1D and the HS model, respectively.

2. Characterization of the 3D isotropic linear viscoelastic behavior

The measurement of the complex modulus of bituminous mixtures has been a central topic in pavement engineering since the 1960s (Papazian, 1962). Nowadays, there is a general consensus on its definition, although its absolute value (or norm) is identified either as the stiffness modulus (CEN, 2012; Di Benedetto et al., 2001) or as the dynamic modulus (AASHTO, 2011; Kim, 2009). Hereafter, we use the term stiffness modulus.

In most practical applications and modelling efforts, the PR of bituminous mixtures is assumed to be time and temperature independent, e.g., $v = 0.35$. It is evident that, for the sake of simplicity, the rheological response in the transverse direction is completely disregarded. In the past 10 years, various experimental studies have shown that v^* of bituminous mixtures is actually a complex number. Its phase angle δ_v is small (generally less than 10°) but not null (Di Benedetto et al., 2007, 2009; Graziani et al., 2014; Nguyen et al., 2009; Pouget et al., 2010). Recently, the RILEM Technical Committee 237-SIB "Testing and characterization of sustainable innovative bituminous materials and systems" organized a round robin test focused on the simultaneous measurement of E^* and v^* of bituminous mixtures. The results confirmed that δ_v is characterized by a typical time and temperature dependence and that the TTSP can be applied for v^* using the same shift factors obtained for E^* (Graziani et al., 2018a; Perraton et al., 2016).

To define and measure the complex PR, a sinusoidal axial test on a cylindrical specimen is considered (Fig. 1). Linearity implies that axial and transverse stress and strains have the same period, whereas isotropy implies that the transverse strain is the same in all directions. Using complex exponentials, stress and strain can be written as follows.

$$\sigma_1(t) = \sigma_{1,0}\sin(\omega t + \delta_1) \rightarrow \sigma_1^*(\omega) = \sigma_{1,0}\exp[j(\omega t + \delta_1)] \tag{1}$$

$$\varepsilon_1(t) = \varepsilon_{1,0}\sin(\omega t) \rightarrow \varepsilon_1^*(\omega) = \varepsilon_{1,0}\exp[j(\omega t)] \tag{2}$$

$$\varepsilon_3(t) = \varepsilon_2(t) = \varepsilon_{2,0}\sin(\omega t - \delta_2) \rightarrow \varepsilon_2^*(\omega) = \varepsilon_{2,0}\exp[j(\omega t - \delta_2)] \tag{3}$$
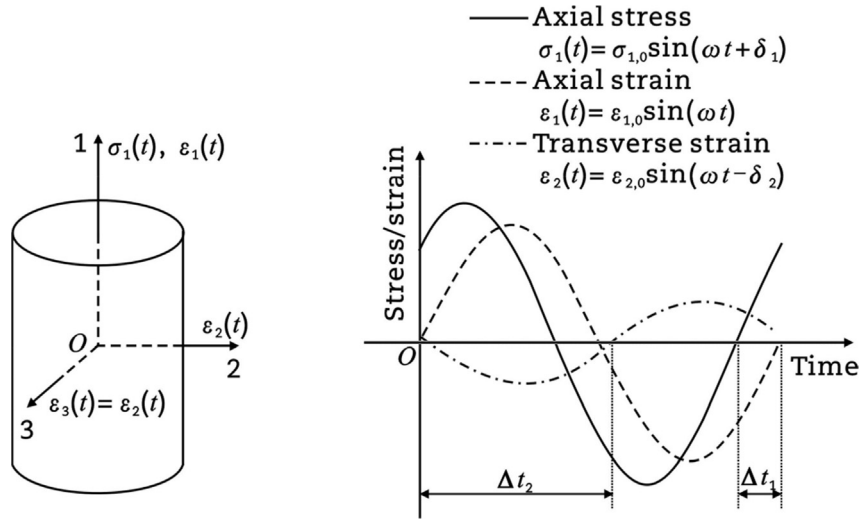
Fig. 1 − **Representation of stress and strain measures during an axial test on an isotropic specimen ($\delta_2 > \pi$).**

where j is the imaginary unit ($j^2 = -1$), $\sigma_{1,0}$, $\varepsilon_{1,0}$ and $\varepsilon_{2,0}$ are the steady-state amplitudes of the sinusoidal signals, $\omega = 2\pi f$ is the angular frequency, f is the testing frequency, δ_1, δ_2 are the phase angles, with respect to the axial strain to which a zero phase is assigned.

The signs of δ_1 and δ_2 in Eqs. (1) − (3) are selected considering that the phase angle is added to indicate a lead and subtracted to indicate a lag (Oppenheim et al., 1996). Therefore, Eq. (1) assumes that axial stress leads axial strain, whereas Eq. (3) assumes that transverse strain lags axial strain. It is important to note that, the first assumption follows from the LVE theory, whereas the second is a heuristic hypothesis (Tschoegl, 1989; Tschoegl et al., 2002). According to this hypothesis, the maximum transverse contraction (or expansion) lags the maximum axial expansion (or contraction) and thus implies $\delta_2 > \pi$, as outlined in Fig. 1.

Fig. 2 shows the complex exponentials described by Eqs. (1) − (3) in the complex plane. In particular, $\delta_2 > \pi$ is depicted in Fig. 2(a), whereas $\delta_2 < \pi$, is depicted in Fig. 2(b). The latter condition implies that the maximum transverse contraction (or expansion) leads the maximum axial expansion (or contraction). It is remarked that this is not in contrast with the LVE theory which only requires that strain lags stress. According to the previous notations, the complex Young's modulus and the complex Poisson's ratio are defined as follows.

$$E^*(\omega) = \frac{\sigma_1^*}{\varepsilon_1^*} = \frac{\sigma_{1,0}}{\varepsilon_{1,0}} \exp(j\delta_1) = E_0 \exp(j\delta_E) \tag{4}$$

$$v^*(\omega) = -\frac{\varepsilon_2^*}{\varepsilon_1^*} = -\frac{\varepsilon_{2,0}}{\varepsilon_{1,0}} \exp(-j\delta_2) = v_0 \exp(-j\delta_v) \tag{5}$$

where $E_0 = \sigma_{1,0}/\varepsilon_{1,0}$, $v_0 = \varepsilon_{2,0}/\varepsilon_{1,0}$ are the absolute values (or norms), $\delta_E = \delta_1$ and $\delta_v = \delta_2 - \pi$ are the phase angles of E^* and v^*, respectively (Fig. 2). In Eq. (5) the negative sign is converted to a π rotation of v^*.

3. Experimental program

3.1. Materials and mixtures

The first mixture tested in this study was a CBTM manufactured in the laboratory using RAP aggregate, reclaimed aggregate, bitumen emulsion and cement. A HMA manufactured at a mixing plant using virgin aggregate, RAP and polymer-modified binder (PMB) was also tested for comparison.

RAP and reclaimed aggregate were sampled from a jobsite located on the A14 Motorway near the city of Ancona, in Italy. The RAP sources were produced by milling the binder and the base courses of the motorway. Both courses were originally manufactured using a PMB. The reclaimed aggregate was produced by milling the underlying cement-treated layer. The virgin aggregate was a 100% crushed limestone. Aggregates were characterized in terms of gradation, particle density, water absorption and bitumen content (only RAP), results are summarized in Table 1.
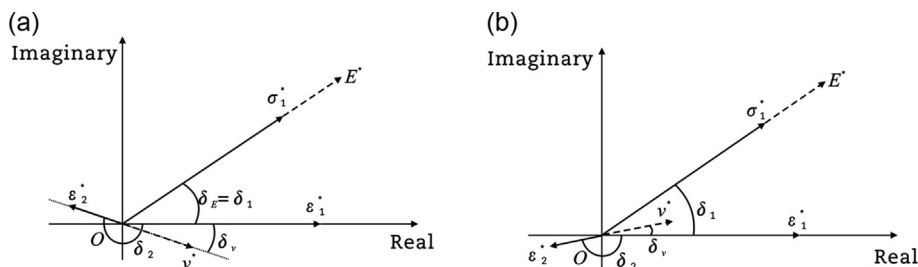

Fig. 2 − **Complex plane representation of stress and strain phasors and response functions E^* and v^*. (a) $\delta_2 > \pi$. (b) $\delta_2 < \pi$.**

J. Traffic Transp. Eng. (Engl. Ed.) 2019; 6 (4): 324–336

327

Table 1 – Physical properties of aggregates.

Material	Water absorption (EN 1097-6) (%)	Particle density (EN 1097-6) (g/cm^3)	Bitumen content (EN 12697-1) (%)
CBTM			
RAP	1.00	2.443	3.59
Reclaimed aggregate	0.90	2.596	–
HMA			
RAP	–	2.667	3.82
Virgin aggregate	–	2.662	–

A cationic bitumen emulsion designated as C 60 B 10 (EN 13808) and a Pozzolanic cement type IV/A (P) with strength class 42.5R (EN 197-1), were used for the CBTM. The PMB used for the HMA contained 3.8% of Styrene-Butadiene-Styrene (SBS) by bitumen weight, its penetration was 71 mm/10 and its softening point was 68 °C.

The aggregate blend used for the CBTM mixture was composed of 50% RAP aggregate and 50% reclaimed aggregate. The dosage of bitumen emulsion was 3.0%, corresponding to 1.8% of fresh bitumen and the dosage of cement was 2.0% (both binders were dosed by dry aggregate mass). The aggregate blend used for the HMA mixture was composed of 75% virgin aggregate and 25% RAP. Its total bitumen content (virgin PMB + PMB from RAP) was equal to 4.8% (by dry aggregate mass). Both aggregate blends had a nominal maximum size of 20 mm, and their gradation was in accordance with the Italian technical specifications for motorway construction (Fig. 3).

3.2. Specimen preparation

The CBTM mixture was prepared according to a job-mix formula previously optimized (Godenzoni et al., 2017). The total water content of the mixture was 5% (by dry aggregate mass), including water from bitumen emulsion and pre-wetting water (Grilli et al., 2012). First, water was added to the dry aggregate blend, then cement and bitumen emulsion were added and samples were mixed with a mechanical mixer, at room temperature. Immediately after mixing, cylindrical specimens were compacted with a gyratory compactor using a mold with diameter of 150 mm, pressure

Fig. 3 – Gradation of aggregate blends for CBTM and HMA mixtures.

of 600 kPa, gyration speed of 30 rpm and angle of inclination of 1.25°. After compaction, CBTM specimens were immediately extracted from the mold and cured for 14 days at 40 °C.

The HMA mixture was sampled at the mixing plant. Cylindrical specimens with a diameter of 150 mm were compacted immediately after sampling by means of a gyratory compactor.

Before mechanical testing, both the HMA and the CBTM specimens were cored to the nominal diameter of 100 mm (Fig. 4). Afterwards, the upper and the lower parts of the specimens were sawed, capped using a two-component resin and then polished, in order to obtain a perfectly smooth surface. The final height and the air voids content of the specimens are reported in Table 2.

3.3. Test setup and data acquisition

The complex Young's modulus and PR were measured performing cyclic compression tests, using a servo-hydraulic press equipped with a temperature-controlled chamber. A haversine load was applied in the axial direction, in control stress mode and a friction reducer (vaseline grease) was used to limit the confining action of the loading platens that alters the uniaxial stress state (Graziani et al., 2014).

Axial and transverse strains were measured using two couples of strain gauges (SG), glued on opposite sides of each specimen at mid-height (Fig. 5). Conventional bonded-wire SG (TML P60) with length of 60 mm and nominal resistance of 120 Ω were employed. A one-component cyanoacrylate adhesive (TML CN-E) was used to glue the SG. Moisture and physical protection was obtained with a butyl rubber covering (TML SB tape) (Fig. 5). The SG were connected using two separate Wheatstone half-bridge circuits for axial and transverse strains. Compensation of temperature effects was obtained with a dummy specimen placed close to the test specimen, inside the temperature-controlled chamber. Signal conditioning, bridge compensation and A/D conversion were carried out using a portable HBM Spider 8 unit. The sampling frequency (f_s) was adapted to the test frequency (f_t) in order to obtain 100 samples per cycle ($f_s = 100\ f_t$). This allowed an effortless data analysis since the same numerical algorithm could be used for all test frequencies.

3.4. Testing program

The testing program consisted of frequency sweeps (12, 4, 1, 0.25 and 0.10 Hz) carried out at six temperatures (0 °C, 10 °C,
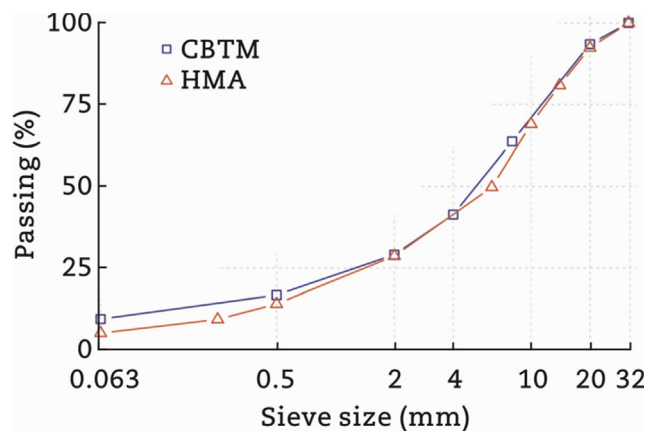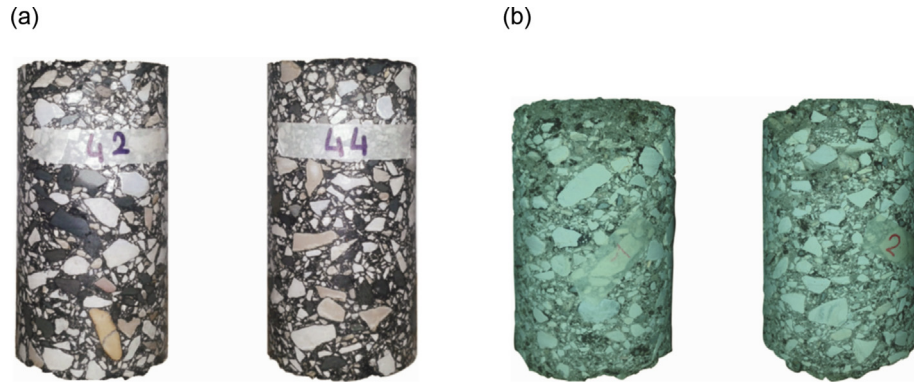
Fig. 4 − Testing specimens after coring, before sawing and capping. (a) HMA. (b) CBTM.

Table 2 − Height and air voids content of the tested specimens.

Mixture	Specimen code	Height (mm)	Air voids (%)
HMA	HMA1	148	3.8
	HMA2	150	4.2
CBTM	CBTM1	132	12.4
	CBTM2	129	12.4

20 °C, 30 °C, 40 °C and 50 °C). The sinusoidal amplitude of the axial strain was 30×10^{-6} m/m for CBTM specimens and 50×10^{-6} m/m for HMA specimens. Testing started from the lower temperature and the higher frequency. Frequency sweeps (20 cycles per frequency) at the same temperature were carried out in the same day (two temperatures per day) and at least 300 s of rest were allowed between two successive frequencies.

3.5. Analysis of time histories

In order to calculate the viscoelastic material functions E^* and v^* (Eqs. (4) and (5)), only the sinusoidal components of the measured stress and strain signals (time-histories), at the testing frequency, shall be considered. Since testing was carried out in cyclic compression, the stress wave was actually the sum of a constant compression (creep component) and a sinusoidal wave. Moreover, since the stress wave was generated using a closed-loop control system, it contained inherent imperfections due to the performance of the testing equipment. Such imperfections result in higher-frequency components superposed to the stress signal. As a consequence, the strain signals contained a non-periodic component, plus additional higher-frequency components which may also originate from nonlinearities in the material response.

The separation of the non-periodic (creep) component from the periodic component of the measured signals, was obtained applying a moving average filter.

$$y_{ma}[n] = \frac{1}{N} \sum_{i=-N/2+1}^{i=N/2} y[n+i] \tag{6}$$

where $y(\cdot)$ is the discrete-time signal (either stress or strain) and $y_{ma}(\cdot)$ is its moving average over one period ($N = 100$). The periodic component $y_p[n]$ is calculated as follows.

$$y_p[n] = y[n] - y_{ma}[n] \tag{7}$$

Then, the third-order Fourier polynomial approximation of the cyclic component was calculated using the equation

$$y_p[n] = \sum_{k=1}^{3} \left[a_k \sin\left(\frac{2\pi k}{N} n\right) + b_k \cos\left(\frac{2\pi k}{N} n\right) \right] + \varepsilon \tag{8}$$

where a_k and b_k are the Fourier coefficients that were estimated using a regression analysis and ε is an error term. It is remarked that, since Eq. (8) is linear in the parameters a_k and b_k, they can be calculated using the closed-form least-squares approach, without numerical approximation. Finally, the amplitude and phase angle of each sinusoidal component were calculated as follows.

$$c_k = \sqrt{a_k^2 + b_k^2} \tag{9}$$

$$\delta_k = \arctan \frac{b_k}{a_k} \tag{10}$$

Only the first harmonic component ($k = 1$) was considered in order to calculate E^* and v^* by means Eqs. (4) and (5). Fig. 6 shows an example of the evolution of E_0, δ_E, v_0 and δ_v for specimen CBTM1 tested at 0.25 Hz and 40 °C. We observe that, even at such high temperature and low frequency, where permanent deformation is supposed to affect the test results, the measured values of E_0 and δ_E are fairly constant throughout the test. This is due to the presence of cement that limits the permanent deformation. The measured values of v_0 and δ_v are more scattered. This can be related to the precision of the measurements and will be further discussed in the next section.

4. Results and analysis

4.1. Analysis of complex Young's modulus

Fig. 7 presents the values E_0 and δ_E measured on specimens HMA1 and CBTM1. As expected, for the HMA mixture, both components show a clear dependency on frequency and temperature. For specimen HMA1, E_0 varies from 431 MPa (50 °C, 0.1 Hz) to 20,547 MPa (0 °C, 12 Hz), while δ_E varies
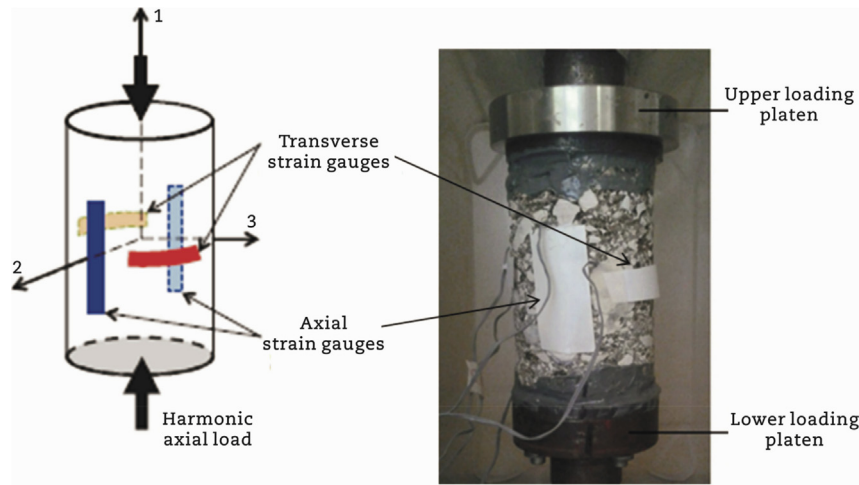
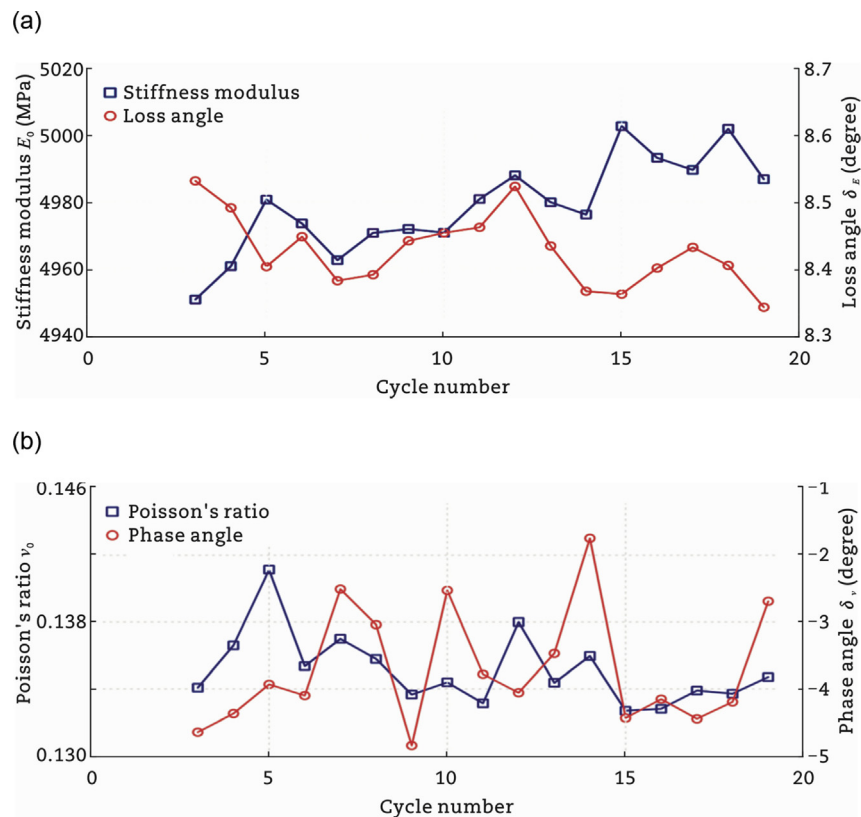**Fig. 5 – Test setup: axial and transverse strain gauges configuration.**

Fig. 6 – Example results for specimen CBTM1 at 0.25 Hz and 40 °C. (a) Evolution of E_0 and δ_E. (b) Evolution of ν_0 and δ_ν.

from 31.7° to 5.4°. We observe the typical temperature and frequency dependence of HMA, in particular at low and intermediate temperatures (from 0 °C to 30 °C) δ_E increases if the test frequency reduces, whereas the opposite behavior is observed at high temperatures (50 °C).

As regards the CBTM mixture, the dependency on frequency and temperature is still present, but not so marked as for HMA. Specifically, for specimen CBTM1, the values of E_0 range from 3151 MPa (50 °C, 0.1 Hz) to 10,519 MPa (0 °C, 12 Hz). We observe that this range of variability is less than one order of magnitude. The values of δ_E range from 12.1° to 3.0°, they decrease if temperature increases and frequency increases.

Fig. 8 presents the values of the complex Young's modulus measured on all the specimens in the Cole-Cole (E_2 vs. E_1) and Black (E_0 vs. δ_E) diagrams. The two couples of specimens give comparable results and the previously observed dependency on frequency and temperature is confirmed. We can conclude that the testing procedure is reliable and that the LVE response of CBTM mixtures can be effectively characterized using the same experimental procedure normally used for HMA. Overall, the thermo-rheological behavior of CBTM and HMA appears to be similar, but for the first material, the variability of both E_0 and δ_E in the tested temperature and frequency range is very limited. We
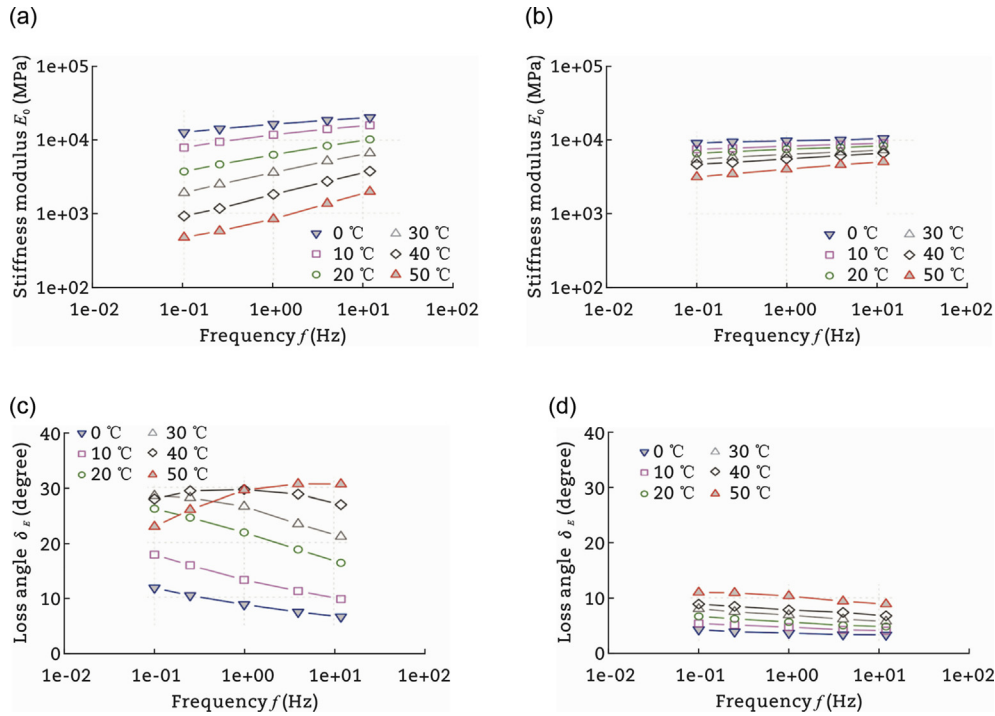
Fig. 7 — Measured values of complex Young's modulus for HMA1 and CBTM1 specimens. (a) E_0 of specimen HMA1. (b) E_0 of specimen CBTM1. (c) δ_E of specimen HMA1. (d) δ_E of specimen CBTM1.
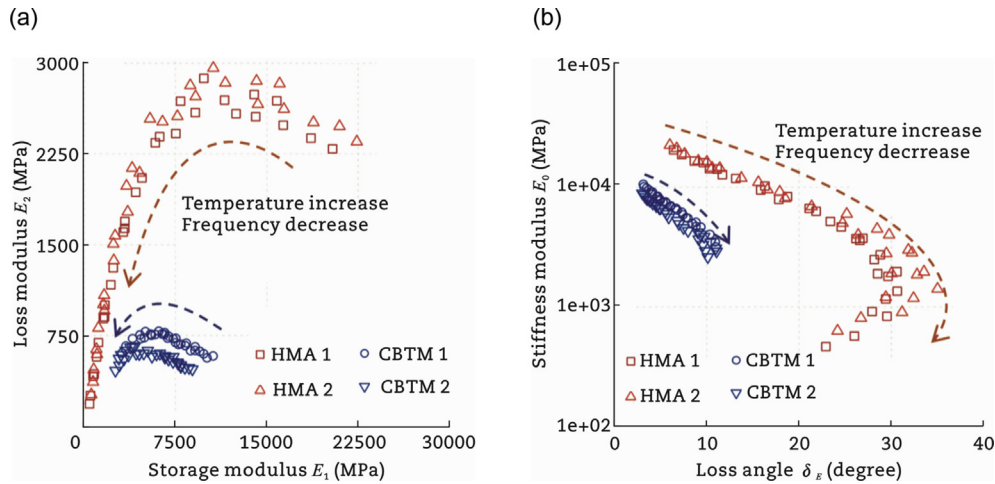

Fig. 8 — Measured values of the complex Young's modulus. (a) Cole-Cole diagram. (b) Black diagram.

highlight that for the CBTM mixture the maximum value of E_0 is much smaller with respect to the HMA mixture, possibly because of their high air void content and low residual bitumen (emulsified bitumen) dosage.

Fig. 8 also shows that unique curves can be used to identify the thermo-rheological behavior of both HMA and CBTM mixtures. This indicates that the TTSP can be applied and allows fitting the E^* values using simple rheological models. The Huet-Sayegh (Sayegh, 1968) and the 2S2P1D analogical models were considered in this study (Olard and Di Benedetto, 2003). The 2S2P1D model features a linear spring in parallel with the series arrangement of a linear spring, two fractional derivative elements (FDE) and a linear dashpot (Fig. 9). It can be described using the following equation.

$$E^*(\omega) = E_e + \frac{E_g - E_e}{1 + d(j\omega\tau)^{-k} + (j\omega\tau)^{-h} + (j\omega\tau\beta)^{-1}} \qquad (11)$$

where E_g and E_e are the glass and equilibrium moduli, respectively, d, k, h are the dimensionless parameters of the FDE elements and τ is the characteristic time. The parameter β can be written as follow.

$$\beta = \frac{\eta}{\tau(E_g - E_e)} \qquad (12)$$

where the parameter η represents the viscosity of the linear dashpot shown in Fig. 9. This linear dashpot was introduced to simulate the behavior of bituminous binders and mixtures at
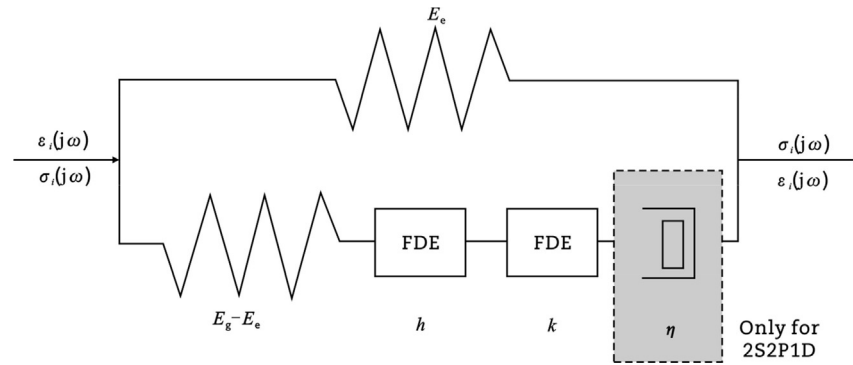
Fig. 9 – Scheme of the Huet-Sayegh and 2S2P1D rheological models.

very low reduced frequencies (high temperatures). In the limiting case $\eta \rightarrow \infty$ the 2S2P1D model reduces to the HS model. In this study, we used the 2S2P1D model for HMA and the HS model for CBTM. The reason is that, even at very low reduced frequencies (high temperatures) the CBTM mixtures showed high values of stiffness and low values of loss angle. This behavior does not envisage any viscous flow and appears to be dominated by cementitious bonds instead of bituminous bonds.

According to the TTST, τ can be written as follow.

$$\tau(T) = a_{T_{ref}}(T)\,\tau_{ref} \tag{13}$$

where T is the testing temperature, $a_{T_{ref}}(T)$ are the shift factors used to describe the temperature dependence of E^* and τ_{ref} is the characteristic time at the reference temperature (T_{ref}). The Williams-Landel-Ferry (WLF) (Williams et al., 1955) equation was considered in this study to simulate the temperature dependence of the shift factors.

$$\log a_{T_{ref}}(T) = \frac{-C_1(T - T_{ref})}{C_2 + (T - T_{ref})} \tag{14}$$

where C_1 and C_2 are empirical constants.

The 2S2P1D, HS and WLF model parameters were calculated using numerical fitting procedures (nonlinear least squares) and are reported in Table 3.

Fig. 10 shows the master curves of E_0 and δ_E at the reference temperature of 0 °C. The shape of the master curves of E_0 for HMA and CBTM is quite different. At high reduced frequencies (low temperatures) the stiffness of HMA is higher than CBTM, whereas the situation is reversed at low reduced frequencies (high temperatures). This difference can also be quantified comparing the values of the glassy and equilibrium moduli (Table 3). The reduced thermorheological sensitivity of the CBTM mixture is due to the

presence of cement and to the low content of fresh bitumen in the mixture (Godenzoni et al., 2015, 2016; Grilli et al., 2013).

The CBTM mixture is characterized by lower values of k and h, with respect to the HMA mixture. These parameters represent the order of derivation of the FDE elements and vary between 0 (the FDE reduces to a spring) and 1 (the FDE reduces to a Newtonian dashpot). Thus, lower values of h and k indicate that in CBTM the elastic component of the material response is proportionally higher than in HMA. This is also consistent with the lower values of the loss angle (Fig. 10(b)). Moreover, the CBTM mixture is characterized by values of τ_{ref} which are about 5 orders of magnitude higher than HMA. This indicates that its loss peak (maximum value of phase angle) is shifted towards very low frequencies and thus its relaxation ability is lower with respect to HMA mixtures.

4.2. Analysis of complex Poisson's ratio

Fig. 11 shows the absolute value v_0 and phase angle δ_v of the complex PR measured on specimens HMA1 and CBTM1. Specimen HMA1, v_0 shows a clear dependency on frequency and temperature (Fig. 11(a)). The minimum value $v_0 = 0.239$ was measured at 0 °C and 12 Hz, whereas the maximum value $v_0 = 0.425$ was measured at 40 °C and 0.1 Hz. Thus, v_0 is higher at lower frequency and higher temperature. At 50 °C the behavior changes because v_0 decreases moving towards lower frequencies. On the other hand, for specimen CBTM1, v_0 is almost independent of temperature and frequency (Fig. 11(b)). The maximum value $v_0 = 0.169$ was measured at 0 °C and 0.25 Hz, whereas the minimum value $v_0 = 0.130$ was measured at 40 °C and 0.1 Hz.

As regards δ_v, the values measured on specimen HMA1 are very small (less than 10°) and mostly positive, except at 50 °C

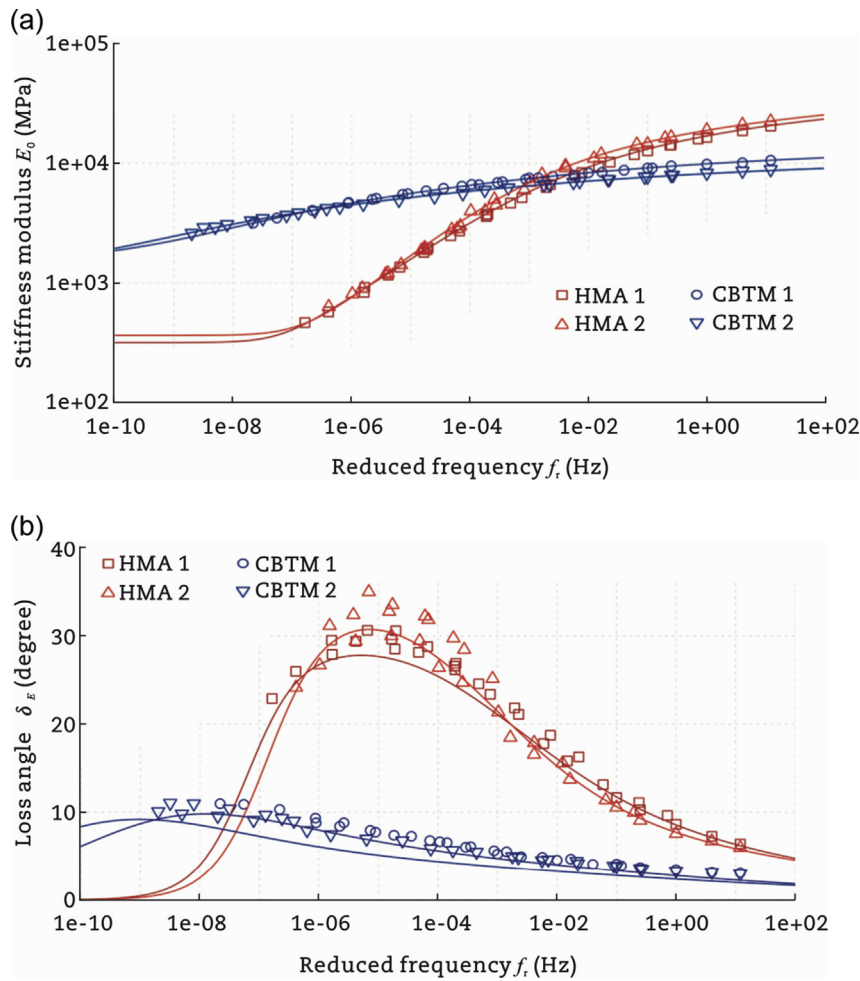| Table 3 – Parameters of the fitted 2S2P1D and WLF models for E* (T_{ref} = 0 °C).									
Specimen	Model	E_g (MPa)	E_e (MPa)	k	h	d	$\log \beta$	$\log \tau_{ref}$	C_1	C_2 (°C)
HMA1	2S2P1D	35,424	316	0.146	0.423	1.858	3.0	1.10	21	141
HMA2	2S2P1D	39,667	363	0.135	0.462	2.001	2.6	1.30	22	140
CBTM1	HS	13,490	1479	0.120	0.390	2.626	–	5.78	11	83
CBTM2	HS	11,074	1259	0.106	0.376	2.626	–	6.75	12	88

Fig. 10 — Young's modulus master curves and 2S2P1D fitted models. (a) Stiffness modulus E_0. (b) Loss angle δ_E.

where two negative values were measured at 0.15 and 0.10 Hz. For specimen CBTM1, the values of δ_v are also very small but mostly negative, with some positive values measured at lower temperatures and higher frequencies. We highlight that, for both mixtures, the variability of δ_v is comparable with its magnitude. This is related to the very small amplitude of the transverse strain. In fact, considering a value $v_0 = 0.15$ and an amplitude of the axial strain $\varepsilon_{1,0} = 30 \times 10^{-6}$ m/m, we obtain an amplitude of the transverse strain $\varepsilon_{2,0} = 4.5 \times 10^{-6}$ m/m, which is very close to the resolution of the measuring system (1×10^{-6} m/m).

Fig. 12 shows the values of the complex PR measured on specimens HMA1 and CBTM1 in the Cole-Cole (v_2 vs. v_1) and Black (v_0 vs. δ_v) diagrams. The arrows superposed to the plots outline the material behavior when temperature increases and frequency decreases. For the specimen HMA1, the lowest value of v_0 (0.2358) was measured at 0 °C and 12 Hz, the corresponding value of δ_v was 3.2° (Fig. 12(b)). We recalled that, according to Eqs. (3) and (5), a positive value of δ_v indicates that the maximum transverse dilation/contraction lags behind the maximum axial contraction/dilation (Fig. 2(a)), which is the expected behavior for a conventional material. In Fig. 12 we also observe that unique curves appear to identify the thermo-rheological behavior of HMA, confirming the validity of the TTSP principle.

The thermo-rheological response of specimen CBTM1 is quite different. A clear dependence on temperature and frequency is not visible, and the validity of the TTSP cannot be confirmed.

Consequently, only the v^* values measured on the HMA specimens can be fitted using the 2S2P1D rheological model.

$$v^*(\omega) = v_e + \frac{v_g - v_e}{1 + d(j\omega\tau_v)^{-k} + (j\omega\tau_v)^{-h} + (j\omega\tau_v\beta)^{-1}} \quad (15)$$

where v_g and v_e are the glass and equilibrium moduli of v^*, respectively, d, k, h and β are dimensionless model parameters and τ_v is the characteristic time. Eq. (15) is analogous to Eq. (11), except that the absolute value of Eq. (15) is a monotonically decreasing function of frequency, whereas the absolute value Eq. (11) is a monotonically increasing function of frequency. Similar to the E* model, τ_v can be written as a function of the testing temperature.

$$\tau_v(T) = a_{T_{ref}}(T) \, \tau_{v,ref} \quad (16)$$

where $a_{T_{ref}}(T)$ are the same shift factors previously determined to describe the temperature dependence of E* and $\tau_{v,ref}$ is the characteristic time at T_{ref}.

Fig. 13 shows the master curves of v_0 and δ_v at $T_{ref} = 0$ °C. In particular, Fig. 13(a) and (c) shows a good agreement between the experimental data and the 2S2P1D model (Table 4). As
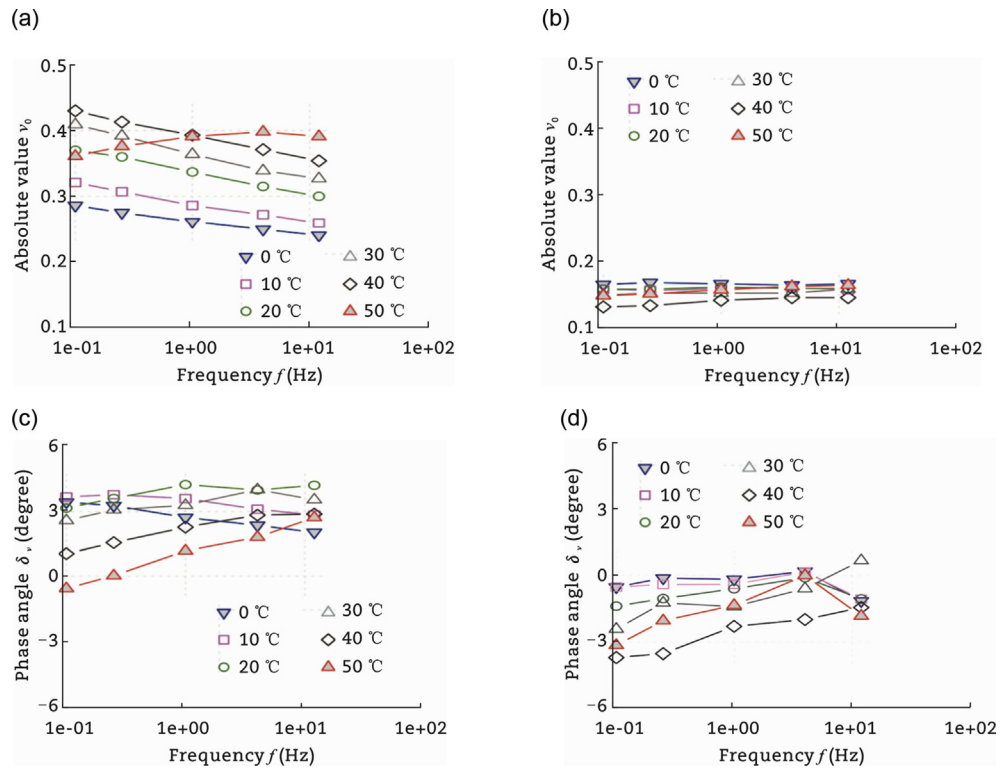
Fig. 11 — Measured values of the complex PR for HMA1 and CBTM1 specimens. (a) v_0 of specimen HMA1. (b) v_0 of specimen CBTM1. (c) δ_v of specimen HMA1. (d) δ_v of specimen CBTM1.
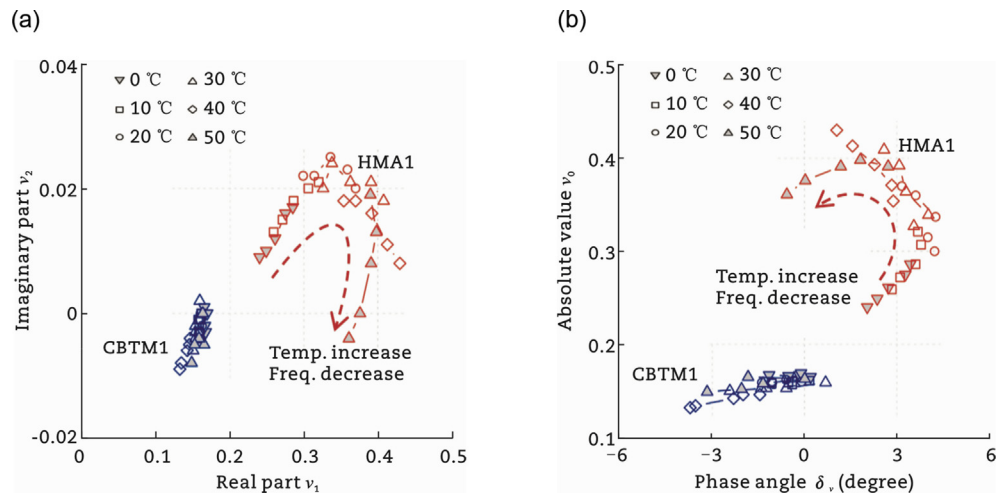

Fig. 12 — Measured values of v^* for specimens HMA1 and CBTM1. (a) Cole-Cole diagram. (b) Black diagram.

regards v_0, the two specimens are characterized by very different maximum values (about 0.42 for HMA1 and 0.72 for HMA2). A similar thermo-rheological behavior in terms of v^* has been previously described in various studies on HMA and, more specifically, values of v_0 greater than 0.5 (the theoretical maximum in isotropic linear elasticity) have been reported by Clec'h et al. (2010), Graziani et al. (2017), Gudmarsson et al. (2015), and Nguyen et al. (2009).

Fig. 13(b) and (d) shows that the thermo-rheological responses of the CBTM specimens are completely different

from HMA specimens. We observe that v_0 is almost constant and that δ_v ranges between about 0° and −3°. Since the three-dimensional characterization of cold mixtures fabricated using bitumen emulsion and cement, is a new subject, there are no similar data available for comparison in the literature. As we previously observed for E^*, certainly cementitious bonds limited the thermo-rheological susceptibility of the CBTM mixture. Indeed, a constant value $v = 0.15$ is normally assumed for cement concrete and cement-treated materials (Huang, 2004) and therefore we
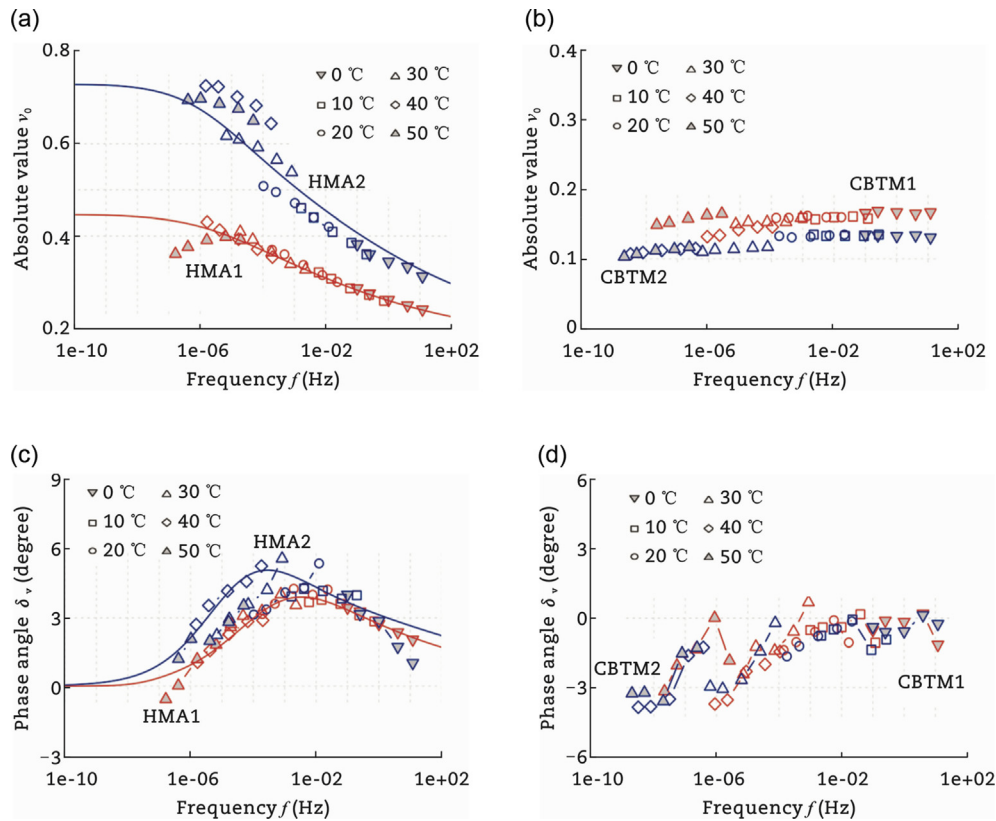
Fig. 13 — Master curves of complex PR. (a) ν_0 for specimens HMA1 and HMA2. (b) ν_0 for specimens CBTM1 and CBTM2. (c) δ_ν for specimens HMA1 and HMA2. (d) δ_ν for specimens CBTM1 and CBTM2.

Table 4 — Parameters of the fitted 2S2P1D model for ν^*.

Specimen	Model	ν_g (MPa)	ν_e (MPa)	k	h	d	$\log \beta$	$\log \tau_{\text{ref}}$
HMA1	2S2P1D	0.20	0.42	0.146	0.423	0.980	2.38	2.36
HMA2	2S2P1D	0.25	0.72	0.135	0.462	1.075	9.64	3.32

conclude that the studied CBTM mixtures show a typical cement-like behavior.

5. Conclusions

In this paper, we analyze the 3D LVE behavior of a cold-recycled CBTM mixture fabricated using bitumen emulsion and cement and containing 50% RAP aggregate and 50% reclaimed aggregate. The behavior of a HMA containing 25% RA and fabricated using polymer-modified binder is also analyzed for comparison.

As regards the HMA mixture, we can conclude that.

- The time—temperature superposition principle is validated for both E^* and ν^* (thermo-rheologically simple behavior in 3D) and the same shift factors can be used for the construction of the master curves of both absolute values (E_0 and ν_0) and phase angles (δ_E and δ_ν).
- The 2S2P1D rheological model correctly simulates the thermo-rheological behavior.
- Despite the use of PMB and 25% RAP, the 3D LVE behavior in terms of E^* and ν^* is similar to that of HMA mixtures produced only with virgin aggregate and pure bitumen.

As regards the CBTM mixture, we can conclude that.

- The thermo-rheological behavior in terms of E^* is similar to that of HMA, in particular, the time—temperature superposition principle is valid and the Huet-Sayegh model can be used to simulate the measured data.
- At high reduced frequencies (low temperatures), the stiffness of CBTM is lower with respect to that of HMA, due to the higher voids and lower fresh bitumen content. On the other hand, at low reduced frequencies (high temperatures) the CBTM is stiffer with respect to the HMA, due to the presence of cementitious bonds.
- The thermo-rheological response in terms of ν^* is very different from that of HMA, in particular, ν_0 is almost constant and very close to 0.15.

Conflict of interests

The authors declare that there is no conflict of interest regarding the publication of this paper.

J. Traffic Transp. Eng. (Engl. Ed.) 2019; 6 (4): 324—336

335

REFERENCES

AASHTO, 2011. Standard Method of Test for Determining Dynamic Modulus of Hot Mix Asphalt (HMA). AASHTO T 342. AASHTO, Washington DC.

Asphalt Academy, 2009. Technical Guideline (TG2): Bitumen Stabilized Materials, second ed. CSIR Built Environment, Pretoria.

Bocci, M., Grilli, A., Cardone, F., et al., 2011. A study on the mechanical behaviour of cement-bitumen treated materials. International Journal of Construction and Building Materials 25 (2), 773—778.

Brown, S.F., Needham, D., 2000. A study of cement modified bitumen emulsion mixtures. Journal of the Association of Asphalt Paving Technologists 69, 92—116.

Clec'h, P., Sauzéat, C., Di Benedetto, H., 2010. Linear viscoelastic behavior and anisotropy of bituminous mixture compacted with a French wheel compactor. In: 2nd International GeoShanghai Conference, Shanghai, 2010.

Comite Europeen de Normalisation (CEN), 2012. Bituminous Mixtures-Test Methods for Hot Mix Asphalt, Part 26: Stiffness. EN 12697-26. CEN, Brussels.

Di Benedetto, H., Partl, M.N., Francken, L., et al., 2001. Stiffness testing for bituminous mixtures. Materials and Structures 34 (2), 66—70.

Di Benedetto, H., Delaporte, B., Sauzeat, C., 2007. Three-dimensional linear behavior of bituminous materials: experiments and modeling. International Journal of Geomechanics 7, 149—157.

Di Benedetto, H., Sauzeat, C., Sohm, J., 2009. Stiffness of bituminous mixtures using ultrasonic wave propagation. Road Materials and Pavement Design 10 (4), 789—814.

Dolzycki, B., Jaczewski, M., Szydlowski, C., 2017. The long-term properties of mineral-cement-emulsion mixtures. Construction and Building Materials 156, 799—808.

Gandi, A., Carter, A., Singh, D., 2017. Rheological behavior of cold recycled asphalt materials with different contents of recycled asphalt pavements. Innovative Infrastructure Solutions 2 (1), 45-45.

Giani, M.I., Dotelli, G., Brandini, N., et al., 2015. Comparative life cycle assessment of asphalt pavements using reclaimed asphalt, warm mix technology and cold in-place recycling. Resources, Conservation and Recycling 104, 224—238.

Godenzoni, C., Graziani, A., Bocci, M., 2015. Influence of reclaimed asphalt content on the complex modulus of cement bitumen treated materials. In: 6th International Conference Bituminous Mixtures and Pavements, Thessaloniki, 2015.

Godenzoni, C., Graziani, A., Perraton, D., 2016. Complex modulus characterisation of cold-recycled mixtures with foamed bitumen and different contents of reclaimed asphalt. Road Materials and Pavement Design 18 (1), 130—150.

Godenzoni, C., Graziani, A., Bocci, M., et al., 2017. Instrumented test section for analyzing the curing process of cold-recycled mixtures. In: 10th International Conference on the Bearing Capacity of Roads, Railways and Airfields (BCRRA 2017), Athens, 2017.

Goyer, S., Dauvergne, M., Wendling, L., et al., 2012. Environmental evaluation of gravel emulsion. In: International Symposium on LCA for Construction Materials, Nantes, 2012.

Graziani, A., Bocci, M., Canestrari, F., 2014. Complex Poisson's ratio of bituminous mixtures: measurement and modeling. Materials and structures 47 (7), 1131—1140.

Graziani, A., Di Benedetto, H., Perraton, D., et al., 2017. Recommendation of RILEM TC 237-SIB on complex Poisson's ratio characterization of bituminous mixtures. Materials and Structures 50 (2), 142-142.

Graziani, A., Di Benedetto, H., Perraton, D., et al., 2018a. Three-dimensional characterisation of linear viscoelastic properties of bituminous mixtures. In: Partl, M., Porot, L., Di Benedetto, H. (Eds.), Testing and Characterization of Sustainable Innovative Bituminous Materials and Systems, Springer, Heidelberg, pp. 127—202.

Graziani, A., Mignini, C., Bocci, E., et al., 2018b. Complex modulus od cold recycled mixtures: measurement and modelling. In: 2018 ISAP Conference, Fortaleza, 2018.

Grilli, A., Graziani, A., Bocci, M., 2012. Compactability and thermal sensitivity of cement—bitumen-treated materials. Road Materials and Pavement Design 13 (4), 599—617.

Grilli, A., Bocci, E., Graziani, A., 2013. Influence of reclaimed asphalt content on the mechanical behaviour of cement-treated mixtures. Road Materials and Pavement Design 14 (3), 666—678.

Gudmarsson, A., Ryden, N., Di Benedetto, H., et al., 2015. Complex modulus and complex Poisson's ratio from cyclic and dynamic modal testing of asphalt concrete. Construction and Building Materials 88, 20—31.

Huang, Y.H., 2004. Pavement Analysis and Design, second ed. Pearson, New York.

Kim, Y.R., 2009. Modeling of Asphalt Concrete. McGraw-Hill Construction, New York.

Nguyen, H.M., Pouget, S., Di Benedetto, H., et al., 2009. Time-temperature super- position principle for bituminous mixtures. European Journal of Environmental and Civil Engineering 13 (9), 1095—1107.

Nikolaides, A., 1994. A new design method for dense cold mixtures. In: The First European Symposium on Performance and Durability of Bituminous Materials, Leeds, 1994.

Olard, F., Di Benedetto, H., 2003. General 2S2P1D model and relation between the linear viscoelastic behaviors of bituminous binders and mixes. Road Materials and Pavement Design 4 (2), 185—224.

Oppenheim, A.V., Willsky, A.S., Nawab, S.H., 1996. Signals and Systems, second ed. Prentice Hall, Upper Saddle River.

Papazian, H.S., 1962. The response of linear viscoelastic materials in the frequency domain with emphasis on asphalt concrete. In: 1st International Conference on the Structural Design of Asphalt Pavements, Ann Arbor, 1962.

Perraton, D., Di Benedetto, H., Sauzéat, C., et al., 2016. 3 Dim experimental investigation of linear viscoelastic properties of bituminous mixtures. Materials and Structures 49 (11), 4813—4829.

Pouget, S., Sauzeat, C., Di Benedetto, H., et al., 2010. From the behavior of constituent materials to the calculation and design of Orthotropic Bridge structures. Road Materials and Pavement Design 11, 111—144.

Sayegh, G., 1968. Viscoelastic properties of bituminous mixtures. In: 2nd International Conference on the Structural Design of Asphalt Pavements, Ann Arbor, 1968.

Sauzeat, C., Di Benedetto, H., 2015. Tridimensional linear viscoelastic behavior of bituminous materials. In: Huang, S.S., Di Benedetto, H. (Eds.), Advances in Asphalt Materials. Woodhead Publishing, Los Angeles, pp. 59—95.

Schwartz, C.W., Diefenderfer, B.K., Bowers, B.F., 2017. Material Properties of Cold In-Place Recycled and Full-Depth Reclamation Asphalt Concrete. NCHRP, Washington DC.

Stimilli, A., Ferrotti, G., Graziani, A., et al., 2013. Performance evaluation of a cold-recycled mixture containing high percentage of reclaimed asphalt. Road Materials and Pavement Design 14 (S1), 149—161.

Thompson, M.R., Garcia, L., Carpenter, S.H., 2009. Cold In-Place Recycling and Full-Depth Recycling with Asphalt Products. Report No. ICT-09-036. Illinois Center for Transportation, Rantoul.

Tschoegl, N.W., 1989. The Phenomenological Theory of Linear Viscoelastic Behavior: an Introduction. Springer, Berlin.

Tschoegl, N.W., Knauss, W., Emri, I., 2002. Poisson's ratio in linear viscoelasticity—a critical review. Mechanics of Time-Dependent Materials 6 (1), 3—51.

Turk, J., Pranjić, A.M., Mladenovič, A., et al., 2016. Environmental comparison of two alternative road pavement rehabilitation techniques: cold-in-place-recycling versus traditional reconstruction. Journal of Cleaner Production 121, 45—55.

Williams, M.L., Landel, R.F., Ferry, J.D., 1955. The temperature dependence of relaxation mechanisms in amorphous polymers and other glass-forming liquids. Journal of the American Chemical Society 77, 3701—3707.

Dr. Carlotta Godenzoni was a PhD student at Università Politecnica delle Marche (Italy), researching the multiscale rheological and mechanical characterization of cold-bituminous recycled materials prepared with bituminous emulsion or foamed bitumen and cement. She currently serves as Airside infrastructure project manager at Bologna Airport (Italy).

Dr. Andrea Graziani is an assistant professor at Università Politecnica delle Marche (Italy). He is interested in cold paving technologies and asphalt emulsion mixtures, three-dimensional characterization of asphalt materials, asphalt pavement reinforcement, asphalt pavement design.

Francesco Canestrari is full professor of roads, railways and airports and chair of the master degree in civil engineering at Università Politecnica delle Marche (Italy). Professor Canestrari is involved as principal investigator in several international research projects. His specialty areas include testing specifications, interface shear characterisation of asphalt layers, reinforced pavements, rheological and performance based characterisation of sustainable and innovative pavement materials.